Theory of the two-loop self-energy correction to the *g* factor in nonperturbative Coulomb fields

B. Sikora,[1,*] V. A. Yerokhin,[1,2] N. S. Oreshkina,[1] H. Cakir,[1] C. H. Keitel,[1] and Z. Harman[1,†]

[1]*Max Planck Institute for Nuclear Physics, Saupfercheckweg 1, D-69117 Heidelberg, Germany*
[2]*Center for Advanced Studies, Peter the Great St. Petersburg Polytechnic University, 195251 St. Petersburg, Russia*

Two-loop self-energy corrections to the bound-electron *g* factor are investigated theoretically to all orders in the nuclear binding strength parameter $Z\alpha$. The separation of divergences is performed by dimensional regularization, and the contributing diagrams are regrouped into specific categories to yield finite results. We evaluate numerically the loop-after-loop terms, and the remaining diagrams by treating the Coulomb interaction in the electron propagators up to first order. The results show that such two-loop terms are mandatory to take into account for projected near-future stringent tests of quantum electrodynamics and for the determination of fundamental constants through the *g* factor.

The *g* factor of one-electron ions can be measured and calculated with exceptional accuracy [1–10]. Its theoretical and experimental values in $^{28}\text{Si}^{13+}$ were found to be in excellent agreement [1]. Since then, experimental uncertainty has decreased by an order of magnitude [2]. Such measurements allowed an improved determination of the electron mass [11] (see also Refs. [12,13]). It is anticipated that, in the foreseeable future, bound-electron *g*-factor measurements will enable an independent determination of the fine-structure constant α [14–16], and an unambiguous extraction of nuclear magnetic momenta [17,18]. To push forward the boundaries of theory, quantum electrodynamic (QED) corrections at the one- and two-loop level need to be calculated with increasing accuracy. One-loop corrections have been evaluated both as a power series in $Z\alpha$ (with Z being the atomic number) and nonperturbatively in this parameter (see, e.g., Refs. [19–21]). Two-loop corrections were evaluated up to fourth order in $Z\alpha$ [19,22]. Contributions of order $\alpha^2(Z\alpha)^5$ were completed recently [10]. At high nuclear charges, where $Z\alpha \approx 1$, an expansion in $Z\alpha$ is not applicable. So far, two-loop diagrams with two electric vacuum polarization (VP) loops and those with one electric VP and one self-energy (SE) loop were evaluated nonperturbatively in $Z\alpha$ [23].

For a broad range of Z, the two-loop SE corrections, which are by far the hardest to calculate, constitute the largest source of uncertainty. This holds true even at $Z = 6$, after a recent high-precision evaluation of the one-loop SE corrections [4,21]. We thus see that higher-order terms in $Z\alpha$ are also necessary at lower nuclear charges, if ultimate precision is required. Therefore, in the current Rapid Communication

we present a theoretical framework for the nonperturbative evaluation of the two-loop SE terms.

There are three two-loop SE diagrams contributing to the *binding energy* of a hydrogenlike ion, namely, the loop-after-loop (LAL), the nested loop (N), and the overlapping loop (O) diagrams. Their calculation has been presented in detail in Refs. [24–30]. The corresponding diagrams for the *g* factor can be generated by magnetic vertex insertions into the Lamb shift diagrams, yielding three nonequivalent diagrams in each of the above classes, shown in Fig. 1.

Basic analysis. We derived formulas for energy shifts induced by each diagram using the two-time Green's function formalism [31]. The corresponding *g*-factor contribution Δg is related to the energy shift by $\Delta E = -\frac{eB}{4m_e}\Delta g$ (in relativistic units), where e and m_e are the electron's charge and mass, respectively, and B is the magnetic field strength.

We begin our analysis with the N and O diagrams. The diagrams with the magnetic field acting on one of the electron propagators inside the SE loops [Figs. 1(e), 1(f), 1(h), and 1(i)] are called vertex diagrams. There are two types of electron propagators the magnetic field can act on: Following the nomenclature of Ref. [24], we call a vertex diagram a "ladder" contribution if the magnetic field acts on the central electron propagator [Figs. 1(e) and 1(h)], and a "side" contribution if the magnetic interaction is connected with the leftmost or rightmost electron propagator [Figs. 1(g) and 1(i)]. The energy shifts corresponding to these diagrams can be written as

$$\Delta E_{\text{ver},i,j} = \langle a|\gamma^0 \Gamma_{ij}^\mu e A_\mu |a\rangle. \tag{1}$$

Here, $i \in \{\text{N, O}\}$ and $j \in \{\text{side, ladder}\}$, $|a\rangle$ denotes the $1s$ reference state, γ^0 is the timelike Dirac matrix, A_μ is the magnetic four-potential with the Lorentz index μ, and the Γ_{ij}^μ are the two-loop vertex functions. The formulas for the latter are lengthy and will be presented elsewhere.

The N and O diagrams in which the magnetic field acts on an external line [Figs. 1(d) and 1(g)] need to be divided into two parts. The electron propagator between the magnetic interaction and the SE loops can be represented as a

---

*bsikora@mpi-hd.mpg.de
†harman@mpi-hd.mpg.de
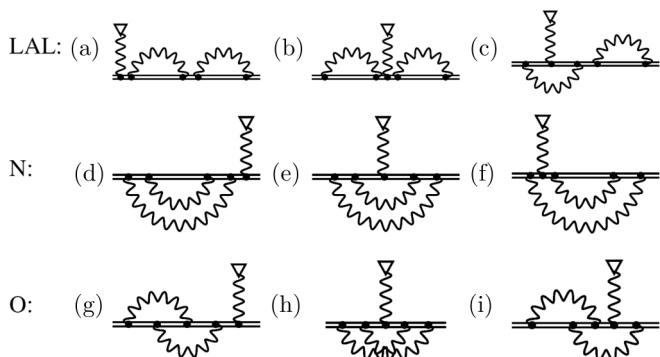
FIG. 1. Furry-picture diagrams of two-loop SE corrections to the *g* factor. Double lines represent electron wave functions or propagators, and the wavy line represents a virtual photon. A wavy line terminated by a triangle represents the interaction with the magnetic field. Loop-after-loop (LAL), nested loop (N), and overlapping loop (O) diagrams are shown in the respective rows.

sum over the spectrum of the Coulomb-Dirac Hamiltonian, $G(E_a) = \sum_n \frac{|n\rangle\langle n|}{E_a - E_n(1-i0)}$, with the E_n being eigenenergies of the eigenstates $|n\rangle$. The cases $E_n \neq E_a$ and $E_n = E_a$ need to be analyzed separately. Following the usual convention in the literature (e.g., Refs. [7,20]), we call these two contributions the irreducible ("irred") and the reducible ("red") parts, respectively. The energy shifts corresponding to these diagrams are

$$\Delta E_{i,\text{irred}} = 2\langle a|\gamma^0 \Sigma_i|\delta_\text{B} a\rangle,$$

$$\Delta E_{i,\text{red}} = \Delta E_{\text{mag}} \langle a|\gamma^0 \left.\frac{\partial \Sigma_i}{\partial E}\right|_{E_a} |a\rangle. \tag{2}$$

Here, the Σ_i are the two-loop SE functions which are discussed in detail in Ref. [24]. $|\delta_\text{B} a\rangle$ is the wave function perturbed by the magnetic field, given as $|\delta_\text{B} a\rangle = \sum_{n \neq a} \frac{|n\rangle\langle n| - e\boldsymbol{\alpha}\cdot\mathbf{A}|a\rangle}{E_a - E_n(1-i0)}$, with $\boldsymbol{\alpha}$ being the usual 3-vector of Dirac matrices. A closed expression for $|\delta_\text{B} a\rangle$ is known [32]. ΔE_{mag} is the energy shift corresponding to the leading *g*-factor diagram [33].

The LAL diagrams [Figs. 1(a)–1(c)] give a large variety of contributions. In Fig. 1(c), a separation into the irreducible and the reducible part needs to be made for the propagator between the two SE loops, similarly to the case of the N and O diagrams. The reducible part can be represented as a product of two one-loop functions, and the irreducible part consists of two one-loop functions connected by a reduced Green's function $G_{\text{red}}(E_a) = \sum_{n, n \neq a} \frac{|n\rangle\langle n|}{E_a - E_n(1-i0)}$. In Figs. 1(a) and 1(b), there are two propagators for which this separation needs to be made. We therefore distinguish between the cases of $E_n \neq E_a$ for both propagators ("irred, irred"), $E_n \neq E_a$ for one propagator and $E_n = E_a$ for the other propagator ("irred, red"), and $E_n = E_a$ for both propagators ("red, red"). The "irred, irred" contributions consist of diagrams with two SE loops connected by G_{red}. The "red, red" contributions can be represented as products of three diagrams, namely, the leading order *g*-factor diagram and two one-loop diagrams. Finally, there are two kinds of "irred, red" contributions. First, there are contributions which can be represented as products of two one-loop diagrams. Second, there are contributions
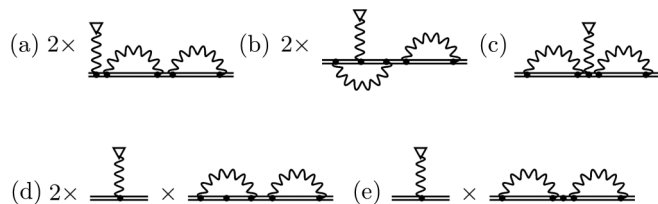
FIG. 2. Two-loop SE diagrams with the loop-after-loop structure ("LAL, irred" contribution). Double lines between two SE loops or between a SE loop and the magnetic interaction represent here the reduced Green's functions. A dot on an electron propagator denotes a derivative with respect to the energy, $\left.\frac{\partial G(E)}{\partial E}\right|_{E=E_a}$.

which can be represented as a product of the leading-order *g*-factor diagram and a diagram which contains two SE loops connected by G_{red}. We cast all LAL contributions into the "LAL, irred" and the "LAL, red" categories, shown in Figs. 2 and 3, respectively.

Regularization of divergences. Self-energy corrections suffer from ultraviolet (UV) divergences, which have to be separated carefully [24]. The standard renormalization method has been elaborated in momentum space for diagrams containing free Dirac propagators, while the Coulomb-Dirac propagators are only known in coordinate space. Therefore, in our regularization scheme we subtract diagrams with the Coulomb-Dirac propagators replaced by propagators containing zero or one interaction with the Coulomb field in such a way that the corresponding difference is rendered UV finite. The subtracted diagrams can then be evaluated in momentum space or in a mixed momentum-coordinate representation. In the case of a one-loop Lamb shift or a one-loop SE correction to the *g* factor, this approach was implemented in Refs. [20,34,35]. In the case of a two-loop SE correction to the *g* factor, one encounters overlapping UV divergences, e.g., the O SE function in Fig. 1(g) consists of two overlapping one-loop vertex functions, each of which gives rise to UV divergences. This property renders the isolation of divergences much more cumbersome.

Furthermore, infrared (IR) divergences may appear whenever the energy of an intermediate state coincides with E_a
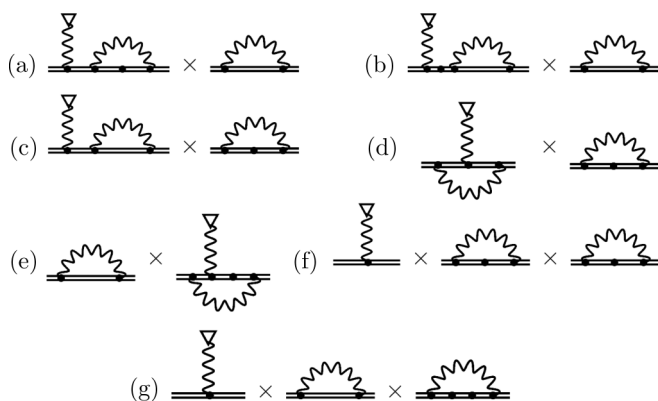
FIG. 3. Reducible two-loop SE diagrams which can be represented as products of one- or zero-loop diagrams ("LAL, red" contribution).

[24]. Such reference-state IR divergences are present in the one-loop g-factor correction as well as in the two-loop Lamb shift. In both cases, it is possible to identify diagrams which are each IR divergent on their own but whose sum is IR finite. The situation for the two-loop SE correction to the g factor is more complicated, requiring an adequate regrouping of different terms. Our analysis of divergences shows a partial cancellation of UV and IR divergences between the different N and O diagrams. The remaining UV and IR divergences in the N and O diagrams are canceled exactly by the divergences in the "LAL, red" contribution. The "LAL, irred" contribution is both UV and IR finite.

Separation into categories. In order to handle divergences, we split all diagrams into different categories. One-loop functions can be split into the zero-, one- (if necessary), and many-potential terms. The zero-potential and, in some cases, the one-potential contributions are UV divergent. These divergent contributions are evaluated in momentum space, using the dimensional regularization procedure [36]. The many-potential functions which are UV finite are computed in coordinate space, as these involve the Coulomb-Dirac propagator. The "LAL, irred" and the "LAL, red" contributions are dealt with using a straightforward generalization of this procedure.

The situation is more complex for the N and O diagrams. While in the one-loop case, diagrams can always be divided into UV-divergent terms, and contributions which contain the Coulomb-Dirac propagator, two-loop diagrams need to be divided into three different categories: (i) diagrams which contain UV divergences, (ii) diagrams which contain the Coulomb-Dirac propagator, and (iii) diagrams which contain both. Using the nomenclature introduced for the two-loop Lamb shift, we refer to these categories as the F, M, and P terms, respectively [29].

Replacing $|\delta_B a\rangle$ with $|a\rangle$ in the "N, irred" and "O, irred" diagrams [Figs. 1(d) and 1(g)], one obtains the known Lamb shift contributions. Therefore, the separation of these diagrams into F, M, and P terms is identical to the case of the Lamb shift [24]. For the N and O reducible and vertex diagrams, we consider the expansion of the electron propagators in powers of the interactions with the nuclear potential and analyze the superficial degree of divergence d, as defined in Ref. [36]. We divide the contributions into F, P, and M terms according to the following definitions,

$$
\begin{aligned}
d \geqslant 0: &\quad \text{F term,} \\
d < 0, &\quad \text{UV-divergent subgraph:} \quad \text{P term,} \\
d < 0, &\quad \text{no UV-divergent subgraph:} \quad \text{M term.}
\end{aligned}
$$

The separation of the "N, vertex" diagrams is illustrated in Fig. 4. The "O, vertex," "O, red," and the "N, red" diagrams can be treated analogously.

Numerical results. In order to assess the relevance of a nonperturbative theory, we evaluate first the F term. This term is expected to be the dominant one as it incorporates the free-electron two-loop SE correction. The calculation typically involves the evaluation of matrix elements of two-loop SE functions which are partially known [24], or in the case of a magnetic insertion, were derived in the current work. Matrix elements are calculated either with Coulomb-Dirac wave functions in coordinate or momentum space, or with the wave function $|\delta_B a\rangle$. Complex γ matrix expressions
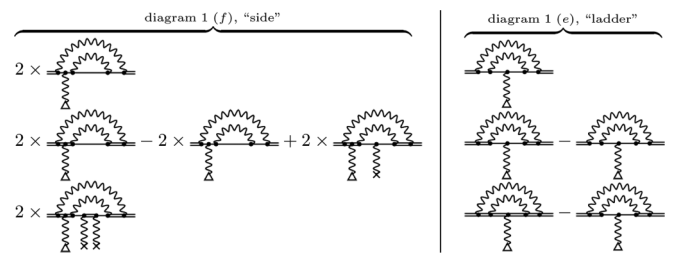
FIG. 4. Separation of the "N, vertex" diagrams [Figs. 1(e) and 1(f)] into F (first line), P (second line), and M terms (third line). A wavy line terminated by a cross represents a Coulomb interaction.

were reduced by computer algebraic methods [37]. Feynman integrals were either carried out analytically, again with the help of symbolic computing [37], or numerically, employing standard or the recently developed extended Gauss-Legendre quadratures [38]. We tested our numerical codes by replacing $|\delta_B a\rangle$ with the regular bound-electron wave function in certain diagrams, reproducing known Lamb shift contributions [24].

For the free-electron case, i.e., in the limit of an infinitesimally weak Coulomb potential, all P and M terms and the one-potential F terms vanish. Furthermore, we expect all "LAL, irred" contributions to converge to zero, as well as those "LAL, red" diagrams which contain the one-loop SE correction [Figs. 3(a), 3(b), 3(e), and 3(g)], or the irreducible one-loop SE wave-function correction to the one-loop g factor [Fig. 3(c)] as a factor.

We define the total zero-potential F-term contribution to consist of the N and O vertex and reducible diagrams, the zero-potential contributions (of both factors) to the "LAL, red" diagrams in Figs. 3(d) and 3(f), and the irreducible zero-potential N and O contributions. The reducible F-term contribution consists of the remaining "LAL, red" diagrams with free internal lines. The one-potential F term consists of the irreducible one-potential N and O contributions. Numerical values and their uncertainties are given in Table I.

TABLE I. The zero-, one-potential, and reducible F and LAL term contributions for different atomic numbers. For $Z \to 0$, $F_{\text{F,0pot}}$ the F term converges to the free-electron limit $F(0) = -0.688\,33\ldots$.

Z	$F_{\text{F,0pot}}$	$F_{\text{F,red}}$	$F_{\text{F,1pot}}$	F_{LAL}
1	$-0.693181(19)$	$0.005715(2)$	$0.00213(27)$	
2	$-0.701989(10)$	$0.015596(2)$	$0.00576(27)$	
3	$-0.712496(9)$	$0.026977(2)$	$0.01011(18)$	
4	$-0.723816(6)$	$0.038885(2)$	$0.014544(44)$	
6	$-0.747062(4)$	$0.062437(2)$	$0.023242(27)$	$0.00026(53)$
8	$-0.769444(6)$	$0.084105(2)$	$0.030852(6)$	$0.00064(53)$
10	$-0.789865(4)$	$0.103024(2)$	$0.037022(16)$	$0.00123(53)$
30	$-0.842748(4)$	$0.132908(9)$	$0.023105(1)$	$0.0196(27)$
40	$-0.781697(4)$	$0.072266(9)$	$-0.015710(1)$	$0.0281(27)$
50	$-0.683620(4)$	$-0.006450(14)$	$-0.066763(1)$	$0.0201(12)$
60	$-0.560628(4)$	$-0.077985(13)$	$-0.134018(2)$	$-0.0252(12)$
70	$-0.419265(4)$	$-0.112472(14)$	$-0.231468(2)$	$-0.1405(12)$
92	$-0.016259(15)$	$0.183186(32)$	$-0.732700(4)$	$-0.9734(39)$
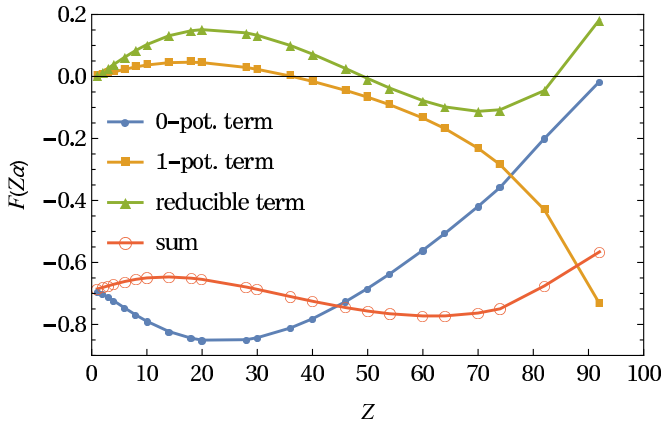
FIG. 5. The zero-, one-potential, and the reducible F-term contributions as a function of Z, expressed in terms of the scaled function $F(Z\alpha)$, defined as $\Delta g = \left(\frac{\alpha}{\pi}\right)^2 F(Z\alpha)$. See text for further details.

FIG. 6. The complete "LAL, irred" contribution, as a function of Z, given in terms of the scaled function $F(Z\alpha)$.

According to the above discussion, we expect the sum of the zero-potential F-term contribution to converge to the free-electron two-loop SE correction for $Z \to 0$. The free-electron g-factor contribution can be determined using the form factors [19], and our results converge well to this value in the low-Z limit (see Fig. 5 and Table I). Figure 5 shows a complex dependence of the calculated F terms on the atomic number Z, which largely deviates from the result of the $Z\alpha$ expansion up to fourth order, highlighting the need for a nonperturbative-in-$Z\alpha$ theory.

In the case of the Lamb shift, the LAL correction gives an estimate of the total two-loop SE correction in a wide Z range [24,30]. To check whether this also holds in our case, we evaluate the LAL g-factor contributions. To this end, it is convenient to define a "SE-perturbed wave function" (see, e.g., Ref. [39]) $|\delta_\Sigma a\rangle = \sum_{n, n \neq a} \frac{|n\rangle\langle n|\Sigma_R|a\rangle}{E_a - E_n}$, with the regularized one-loop SE operator Σ_R. The most difficult aspect of the LAL calculation is the numerical determination of $|\delta_\Sigma a\rangle$, for which we used the B-spline method [40,41]. The g-factor contribution corresponding to Fig. 2(e) is $\Delta g_{LAL,e} = -g_D\langle\delta_\Sigma a|\delta_\Sigma a\rangle$. The computation of Fig. 2(c) is similar to the formula for the computation of the Dirac value $g_D = -\frac{8m_e}{3}\int_0^\infty dr\, r^3 f_a(r) g_a(r)$, with the radial components $g_a(r), f_a(r)$ of the usual wave function replaced by those of $|\delta_\Sigma a\rangle$. The remaining LAL diagrams can be rewritten as matrix elements of the one-loop SE or vertex functions, with either the usual wave function or $|\delta_B a\rangle$ on one side and $|\delta_\Sigma a\rangle$ on the other side. The one-loop operator has to be expanded into zero-, one- (if necessary), and many-potential terms. Numerical results for the total "LAL, irred" contribution are given in the last column of Table I and shown in Fig. 6. Unlike in the case of the Lamb shift, in the g factor the F terms dominate due to the nonvanishing free-electron limit up to high Z values. Figure 6 demonstrates that the behavior of the "LAL, irred" term at intermediate and high Z largely deviates from its low-Z characteristics, and it
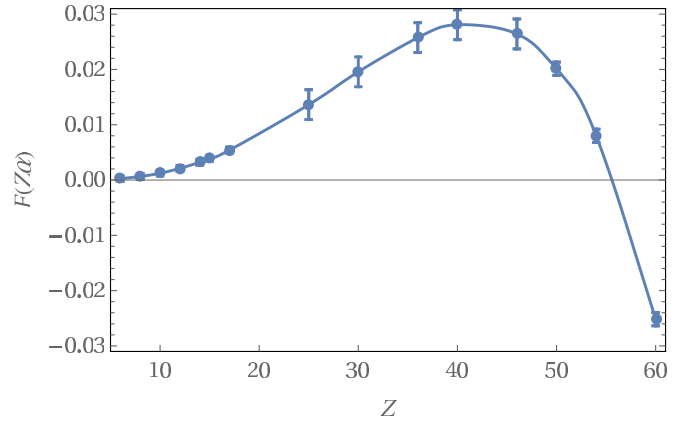
even changes sign around $Z = 55$. A highly nonperturbative behavior of the LAL term was also observed in Lamb shift calculations [30].

In order to ascertain the significance of our numerical calculations, we compared the numerical uncertainties of the evaluated contributions with the unknown higher-order two-loop effects, estimated in Ref. [10] based on the expansion in $Z\alpha$. We found that, for $Z = 30$, both uncertainties are approximately 1.5×10^{-8}, while for $Z \geqslant 40$, our uncertainties are significantly smaller than the ones estimated in Ref. [10]. We therefore conclude that our all-order calculations will enable a significant improvement of the theoretical accuracy of the g-factor of high-Z ions, provided the M- and P-term contributions can be evaluated with an accuracy comparable to that of the LAL contributions.

Summary. The theoretical framework for the evaluation of two-loop SE corrections to the g factor in a nonperturbative nuclear field has been developed. The isolation of divergences was carried out by separating the LAL, N, and O Furry-picture diagrams into terms consisting of diagrams with UV divergences, diagrams which contain a Coulomb-Dirac propagator, and diagrams which contain both. Such a rearrangement assures finite results. Numerical results are given for the dominating group of terms, the F terms, namely, those in which the interaction of the nucleus in the intermediate states is treated up to first order, and for the LAL diagrams. The results show that a nonperturbative treatment is essential in a rigorous description of the bound-electron g factor, and will be relevant to projected tests of QED in strong Coulomb fields and to the determination of α [14,42] in planned experiments with highly charged ions [42].

[1] S. Sturm, A. Wagner, B. Schabinger, J. Zatorski, Z. Harman, W. Quint, G. Werth, C. H. Keitel, and K. Blaum, Phys. Rev. Lett. **107**, 023002 (2011).

[2] S. Sturm, A. Wagner, M. Kretzschmar, W. Quint, G. Werth, and K. Blaum, Phys. Rev. A **87**, 030501(R) (2013).

[3] K. Pachucki, U. D. Jentschura, and V. A. Yerokhin, Phys. Rev. Lett. **93**, 150401 (2004).

[4] K. Pachucki and M. Puchalski, Phys. Rev. A **96**, 032503 (2017).

[5] V. A. Yerokhin, P. Indelicato, and V. M. Shabaev, Phys. Rev. Lett. **89**, 143001 (2002).

[6] V. M. Shabaev and V. A. Yerokhin, Phys. Rev. Lett. **88**, 091801 (2002).

[7] T. Beier, Phys. Rep. **339**, 79 (2000).

[8] S. G. Karshenboim, V. G. Ivanov, and V. M. Shabaev, J. Exp. Theor. Phys. **93**, 477 (2001).

[9] R. N. Lee, A. I. Milstein, I. S. Terekhov, and S. G. Karshenboim, Phys. Rev. A **71**, 052501 (2005).

[10] A. Czarnecki, M. Dowling, J. Piclum, and R. Szafron, Phys. Rev. Lett. **120**, 043203 (2018).

[11] S. Sturm, F. Köhler, J. Zatorski, A. Wagner, Z. Harman, G. Werth, W. Quint, C. H. Keitel, and K. Blaum, Nature (London) **506**, 467 (2014).

[12] H. Häffner, T. Beier, N. Hermanspahn, H.-J. Kluge, W. Quint, S. Stahl, J. Verdú, and G. Werth, Phys. Rev. Lett. **85**, 5308 (2000).

[13] J. Verdú, S. Djekić, H. Haffner, S. Stahl, T. Valenzuela, M. Vogel, G. Werth, H.-J. Kluge, and W. Quint, Phys. Rev. Lett. **92**, 093002 (2004).

[14] V. M. Shabaev, D. A. Glazov, N. S. Oreshkina, A. V. Volotka, G. Plunien, H.-J. Kluge, and W. Quint, Phys. Rev. Lett. **96**, 253002 (2006).

[15] V. A. Yerokhin, E. Berseneva, Z. Harman, I. I. Tupitsyn, and C. H. Keitel, Phys. Rev. Lett. **116**, 100801 (2016).

[16] I. Arapoglou, A. Egl, M. Höcker, T. Sailer, B. Tu, A. Weigel, R. Wolf, H. Cakir, V. A. Yerokhin, N. S. Oreshkina *et al.*, Phys. Rev. Lett. **122**, 253001 (2019).

[17] V. A. Yerokhin, K. Pachucki, Z. Harman, and C. H. Keitel, Phys. Rev. Lett. **107**, 043004 (2011).

[18] S. Schmidt, J. Billowes, M. L. Bissell, K. Blaum, R. F. G. Ruiz, H. Heylen, S. Malbrunot-Ettenauer, G. Neyens, W. Nörtershäuser, G. Plunien *et al.*, Phys. Lett. B **779**, 324 (2018).

[19] K. Pachucki, A. Czarnecki, U. D. Jentschura, and V. A. Yerokhin, Phys. Rev. A **72**, 022108 (2005).

[20] V. A. Yerokhin, P. Indelicato, and V. M. Shabaev, Phys. Rev. A **69**, 052503 (2004).

[21] V. A. Yerokhin and Z. Harman, Phys. Rev. A **95**, 060501(R) (2017).

[22] A. Czarnecki and R. Szafron, Phys. Rev. A **94**, 060501(R) (2016).

[23] V. A. Yerokhin and Z. Harman, Phys. Rev. A **88**, 042502 (2013).

[24] V. A. Yerokhin, P. Indelicato, and V. M. Shabaev, Eur. Phys. J. D **25**, 203 (2003).

[25] V. A. Yerokhin, P. Indelicato, and V. M. Shabaev, Phys. Rev. Lett. **91**, 073001 (2003).

[26] V. A. Yerokhin, P. Indelicato, and V. M. Shabaev, Phys. Rev. Lett. **97**, 253004 (2006).

[27] V. A. Yerokhin, Eur. Phys. J. D **58**, 57 (2010).

[28] V. A. Yerokhin, Phys. Rev. A **97**, 052509 (2018).

[29] S. Mallampalli and J. Sapirstein, Phys. Rev. A **57**, 1548 (1998).

[30] S. Mallampalli and J. Sapirstein, Phys. Rev. Lett. **80**, 5297 (1998).

[31] V. M. Shabaev, Phys. Rep. **356**, 119 (2002).

[32] V. M. Shabaev, in *Precision Physics of Simple Atomic Systems*, edited by S. G. Karshenboim and V. B. Smirnov (Springer, Berlin, 2003), pp. 97–113.

[33] G. Breit, Nature (London) **122**, 649 (1928).

[34] N. J. Snyderman, Ann. Phys. (NY) **211**, 43 (1991).

[35] V. A. Yerokhin and V. M. Shabaev, Phys. Rev. A **60**, 800 (1999).

[36] M. E. Peskin and D. V. Schroeder, *An Introduction to Quantum Field Theory* (Westview Press, Boulder, CO, 1995).

[37] S. Wolfram, *Mathematica–A System for Doing Mathematics by Computer* (Addison-Wesley, Boston, 1991).

[38] K. Pachucki, M. Puchalski, and V. Yerokhin, Comput. Phys. Commun. **185**, 2913 (2014).

[39] J. Holmberg, A. N. Artemyev, A. Surzhykov, V. A. Yerokhin, and T. Stöhlker, Phys. Rev. A **92**, 042510 (2015).

[40] W. R. Johnson, S. A. Blundell, and J. Sapirstein, Phys. Rev. A **37**, 307 (1988).

[41] V. M. Shabaev, I. I. Tupitsyn, V. A. Yerokhin, G. Plunien, and G. Soff, Phys. Rev. Lett. **93**, 130405 (2004).

[42] S. Sturm, M. Vogel, F. Köhler-Langes, W. Quint, K. Blaum, and G. Werth, Atoms **5**, 4 (2017).